ECCOMAS Congress 2016
VII European Congress on Computational Methods in Applied Sciences and Engineering
M. Papadrakakis, V. Papadopoulos, G. Stefanou, V. Plevris (eds.)
Crete Island, Greece, 5–10 June 2016

STRENGTH AND WEIGHT EQUIVALENT SUBSTITUTION OF LARGE SANDWICH PANELS BY MONOLITHIC CFRP STRUCTURES

Martin Meindlhumer[1,2] **and Martin Schagerl**[2]

[1]Johannes Kepler University Linz
Institute of Constructional Lightweight Design
Linz, Austria
e-mail: martin.meindlhumer_1@jku.at, martin.schagerl@jku.at

[2] FACC Operations GmbH
Research and Development
Ried im Innkreis, Austria
e-mail: martin.meindlhumer@facc.com

Keywords: Aircraft Structures, Composite Structures, Sandwich Structures, Control Surfaces, Alternative Design Philosophies, Shell Structures, Buckling

Abstract. *A general trend in the aircraft industry is to replace sandwich structures made from fiber-polymer-composites and low-density honeycomb cores by monolithic structures entirely made from fiber-polymer-composites. The fields of applications addressed here are primary and secondary control surfaces of civil aircraft wings and stabilizers. However, they can be directly extended to other applications. The main motivation for such a substitution is to reduce manufacturing efforts. For honeycomb sandwich designs mainly resin pre-impregnated fiber semi-finished products are applied and often the structures are built and cured in an autoclave in one or several steps. This is cost intensive. Thus, resin infusion technology is an attractive alternative. Dry fibers are saturated with resin during the curing process by applying vacuum. Here, just an oven is required. Another reason is that sandwich structures used on aircraft are exposed to large varying environmental conditions. Condensation and absorption of water can cause an increase in the total mass and once the water is frozen, serious damages may occur. Other advantages include ease in detection of structural damages and manufacturing defects and reduction in repair efforts. Control surface structures are loaded by pressure distributions over their surfaces. The sandwich design is optimal to withstand bending moments, shear forces and torsional moments. The challenge is to keep the mass, when the design is changed to monolithic.*

This contribution presents two design alternatives, one developed on top of the other, which allow the manufacturing of monolithic highly integrated laminated structures within one layup and curing step. Additionally, aerodynamic properties are guaranteed on the top and the bottom of the control surface. A reference structure is derived from a state-of-the-art spoiler, which is equipped with a honeycomb core. This structure is then compared with the alternative design proposed.

1 INTRODUCTION

A general trend in the aircraft industry is to replace sandwich structures by monolithic structures. In the context to this work a sandwich structure is built by a lower and upper skin made from layers of fiber-reinforced-polymers and a honeycomb core in between. A monolithic structure is entirely made from composite layers. The fields of applications addressed here are primary and secondary control surfaces of civil aircraft wings and stabilizers, but they can be extended to other applications directly. There are several reasons motivating such a substitution. One is simply to reduce the manufacturing efforts. Honeycomb cores require the use of resin pre-impregnated fiber products. The sandwich structure has to be cured in one or several steps in an autoclave, where defined pressures and temperatures are applied in a nitrogen-filled environment. This process is cost intensive. Another reason is their behavior during their operating life. Sandwich structures as used on an aircraft are exposed to large varying environmental conditions, which may cause negative implications. One example is the condensation of water, which can be absorbed by the aramid honeycomb core. Despite the mass increase, the absorbed water may freeze and cause serious damage to the sandwich structure. Monolithic structures will allow the application of alternative, more cost efficient manufacturing process technologies like resin infusion. Here, dry fiber products are saturated with resin during the curing process by applying vacuum. This approach is cheaper, because just an oven is required. An increased level of automation is given. In addition, the service life is better controllable in respect to maintenance and repair. Other advantages include ease in detection of structural damages and manufacturing defects and reduction in repair efforts.

Control surface structures are loaded by pressure distributions acting on their surfaces. The sandwich design is, from the structural point of view, optimal to withstand bending moments, shear forces and torsional moments. The challenge is to keep the weight, when the design is changed to monolithic. In addition, aerodynamic properties, which are needed on the top and the bottom surfaces, increase the demand for design solutions which are simpler to manufacture. This contribution presents and discusses two alternative design approaches, which allow the fabrication of monolithic highly integrated laminated structures within one layup and curing step. Compared to [1], the approaches are developed under analytic considerations on the basis of a simplified geometry derived from an aircraft spoiler, which is equipped with a honeycomb core. First, this sandwich reference structure is analyzed for static displacements and occurring stresses. Its weight is calculated. Second, two design alternatives are presented and analyzed. The latter one is derived from the drawbacks of the first one. Finally, the results are justified with the analysis data of the sandwich reference structure and a conclusion is drawn.

2 AIRCRAFT SPOILER AS CASE EXAMPLE

An aircraft spoiler is a typical representative of control surfaces where the sandwich design is state of the art. Spoilers are often multifunctional. Immediately after landing, or in an event of an aborted take-off, they are deflected in an almost upright position. As a result of the interrupted airflow over the flaps, the wing loses a large part of its lift, which increases the normal force on the tires and makes breaking more effective. In addition, they create considerable drag and these combined effects increase the deceleration up to 20%. Outboard spoilers may be used in flight when an appreciable increment of drag is required to obtain a high rate of descent or improved speed stability with a constant angle of decent[2]. In the present work the design and functionality of an aircraft wing spoiler is transferred to a simplified analysis model more suitable for the purpose of the current demonstration. However, the work presented in the

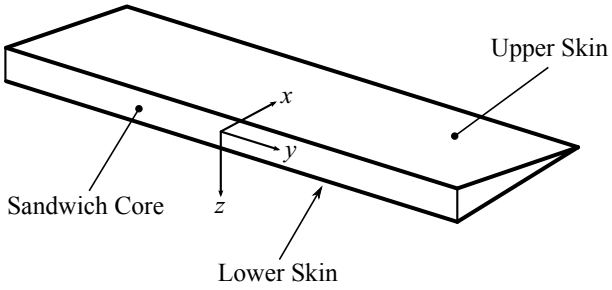

Figure 1: Simplified geometry of an aircraft control surface.

E_{11}	E_{22}	ν_{12}	ρ	CPT	R^t_{11}	R^c_{11}	R^t_{22}	R^c_{22}	R_{12}
154	8.5	0.35	1.58	0.127	2610	1450	55	285	105
GPa	GPa	-	$\mathrm{g/cm^3}$	mm	MPa	MPa	MPa	MPa	MPa

Table 1: Material data of the unidirectional carbon fiber epoxy resin tape.

following can be extended straightforwardly to other control surface structures and to various applications.

2.1 A simplified sandwich structure for reference

The reference design is based on the overall dimensions, material data, loads and boundary conditions of a state-of-the-art aircraft spoiler. Thus, a simplified problem, but of similar scale is investigated. In Fig. 1 the simplified geometry, their components and its position in the Cartesian coordinate system is presented. Its overall geometric dimensions are $2400 \times 800 \times 120$ mm. The base surface of the triangular prism is coplanar to the yz-plane of the defined coordinate system. The structure is symmetrical about the xy-plane and the xz-plane. Unless otherwise stated, the structure is presented in the shown position in the following. The laminate of the lower and upper skin is produced by unidirectional tapes of epoxy resin-impregnated carbon fibers stacked in the sequence of $(45°/\text{-}45°/90°)_s$, where the $0°$-direction points in the x-direction. An aramid honeycomb is selected for the sandwich core. Its ribbon direction is aligned with the y-axis. The corresponding shear strength is higher in this direction compared to the perpendicular one. The material properties and strength allowable of the carbon epoxy tape and the honeycomb core are provided in Tab. 1 and 2, respectively. The axes of the local material coordinate systems are named as 11 (in fiber direction for the carbon plies or ribbon direction of the honeycomb core), 22 (in-plane transverse fiber direction or ribbon direction) and 33 (out-of-plane transverse fiber direction or ribbon direction). Accordingly, shear directions are defined with the indices 12, 23 and 13. The superscripts c and t indicate compression and tension, respectively. The core and the skins are bonded together with film adhesive. However, the structural behavior of the adhesive joint is not considered in this study, as a perfect binding at material interfaces being assumed. For mass calculation, the adhesive density is given as $250\ \mathrm{g/m^2}$.

Despite the generality in practical application of the presented design approaches, the boundary conditions are particularly specified. Here, air loads acting on the upper skin are transferred to the wing structure via three stiff metal brackets located at the center and each corner. In contrast to air suction-up loads in retracted position, pressure loads occur when the spoiler is in extended position immediately after landing, which is the most critical loading situation. As

E_{11}	E_{22}	E_{33}	G_{12}	G_{23}	G_{13}	ρ	S_{33}^c	S_{13}	S_{23}
1	1	138	1	19	31	0.048	1.24	0.98	0.5
MPa	MPa	MPa	MPa	MPa	MPa	$\mathrm{g/cm^3}$	MPa	MPa	MPa

Table 2: Material data of the aramid honeycomb core.

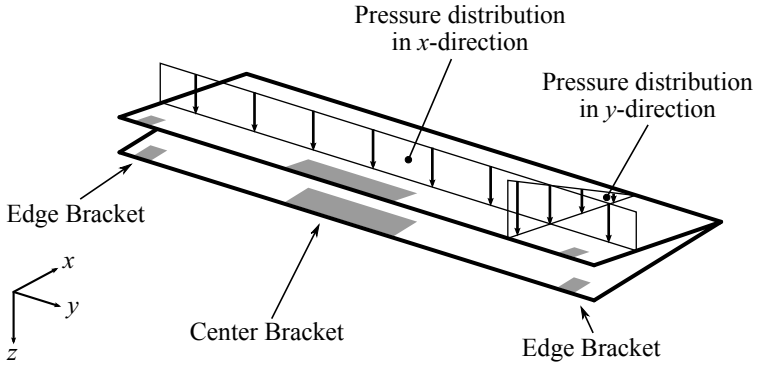

Figure 2: Schematic sketch of the applied pressure field and the bracket locations, where the structure is constrained.

shown in Fig. 2, the pressure is triangular distributed in x-direction with its maximum at the leading edge ($x = 0$) and rectangular in y-direction. The triangular distribution originates from spoiler extension. The rectangular one comes from the assumption, that the neighboring spoilers are in extended mode as well. Two load cases are considered. In the first case, the structure is intact. All degrees of freedom of the nodes at the two locations named center bracket in Fig. 2 are constraint. The nodes at the edge brackets are constraint in z-direction only. A maximum pressure of $0.0345\ \mathrm{N/mm^2}$, which represents the ultimate load, is applied. In the second case, one or both of the edge brackets failed. Therefore, the constraints of the nodes at the edge bracket locations are released. In consideration of sub-component failure only the limit loads are applied, which are 1.5 times lower than ultimate loads. Thus, the maximum acting pressure is $0.023\ \mathrm{N/mm^2}$. Details of the definition of limit load and ultimate load can be found in the EASA Certification specifications for large airplanes in chapter 25.301 and 25.302 [3].

The Finite Element discretization of the lower skin, upper skin and the alternative design features proposed in the following sections is utilized with standard first-order shell elements. The mesh of the honeycomb core in the reference sandwich design is built with first-order hexahedral elements. The average edge length of the volume and shell elements is $20\ \mathrm{mm}$. For pre- and post-processing the commercial software HyperWorks 13.0 (Altair Engineering Inc., Troy, MI, USA) is applied. The FEM simulations are carried out using the commercial solver OptiStruct (Altair Engineering Inc., Troy, MI, USA).

2.2 The structural behavior of the sandwich design

The sandwich structure described above is investigated regarding its deformation and regarding the stresses in the plies and the honeycomb core. Reserve factors are calculated from the materials resistance values (strength allowables) and finally, the structural mass is calculated. The absolute displacement plots for load cases 1 and 2 are shown in Fig. 3. To compare this design to the following ones, three, for the global displacement characteristic nodes are selected. Their absolute displacement values can be found in Tab. 4. The maximum in-plane ply stresses

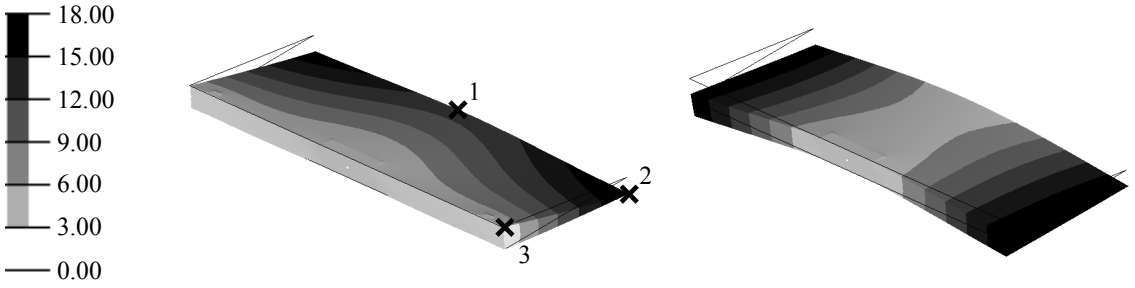

a) Load Case 1 b) Load Case 2

Figure 3: Absolute displacement plot of the sandwich reference structure for a) load case 1 and b) load case 2 in [mm], scale factor: 10, markings show the 3 characteristic nodes for further evaluation.

occurring for load cases 1 and 2 are summarized in Tab. 5. The stresses in the honeycomb core shall be considered as well. Here, the maximum stress values are

$$\sigma_{33}^{c} = 0.2\text{MPa} \qquad \sigma_{13} = 0.4\text{MPa} \qquad \sigma_{23} = 0.3\text{MPa}$$
$$\sigma_{33}^{c} = 0.1\text{MPa} \qquad \sigma_{13} = 0.4\text{MPa} \qquad \sigma_{23} = 0.2\text{MPa}$$

for load cases 1 and 2, respectively, where the elements next to the constraint nodes are not considered. Reserve factors are calculated to show the overall static strength of the structure. For the carbon plies the maximum stress first ply failure criteria

$$RF_{ij}^{(c,t,\text{-})} = \frac{R_{ij}^{(c,t,\text{-})}}{\sigma_{ij}^{(c,t,\text{-})}} \tag{1}$$

is applied [4] for the maximum in-plane stresses summarized in Tab. 5. The reserve factors are given in Tab. 6. The material allowables are taken from Tab. 1. The systematic application of (1) yields the reserve factors for the honeycomb for load cases 1 and 2, respectively

$$RF_{33}^{c} = 6.2 \qquad RF_{13} = 3.3 \qquad RF_{23} = 1.3$$
$$RF_{33}^{c} = 12.4 \qquad RF_{13} = 4.9 \qquad RF_{23} = 1.3$$

Finally, the total mass of the sandwich reference design calculated from the individual mass densities of the components is given in Tab. 7. The data generated from the reference design is used to be compared with those of the alternative designs developed in the following section.

3 DESIGN ALTERNATIVES AND THEIR STRUCTURAL ANALYSES

The result of the above investigated sandwich structure reveals that the dominating global reactions to the given loading situations are bending around the x-axis and bending around the y-axis (see Fig. 1). The honeycomb core has the function of keeping the distance between the bottom and top laminates. However, a further main task is to resist the acting shear stresses with a minimum of structural mass. The substitution of the honeycomb core requires design features that are able to carry the shear stresses. In the following, two alternative designs are presented, which might be able to substitute the honeycomb core. In general, the same carbon epoxy ply material and film adhesive (if needed) are applied. The standard layup of the lower and upper skin is kept, but extended by additional layers as necessary. The load cases and boundary conditions are identical to that of the sandwich structure.

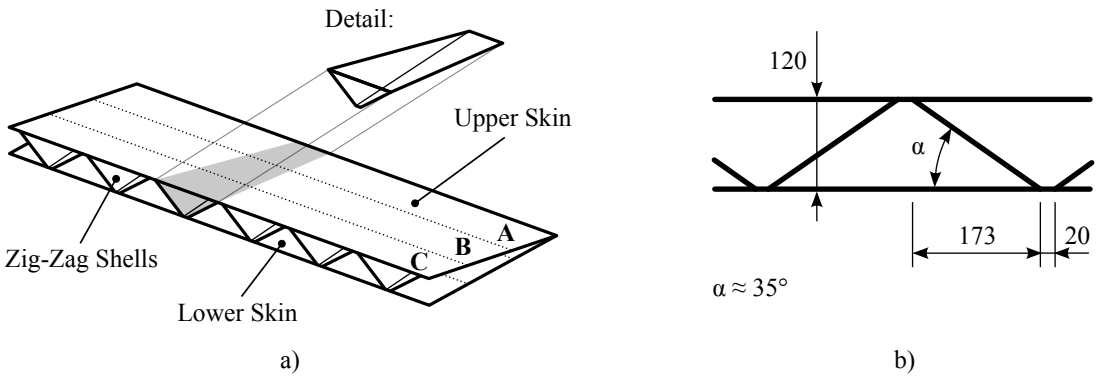

Figure 4: Monolithic box with a) zig-zag stiffeners and b) its local dimensions in [mm].

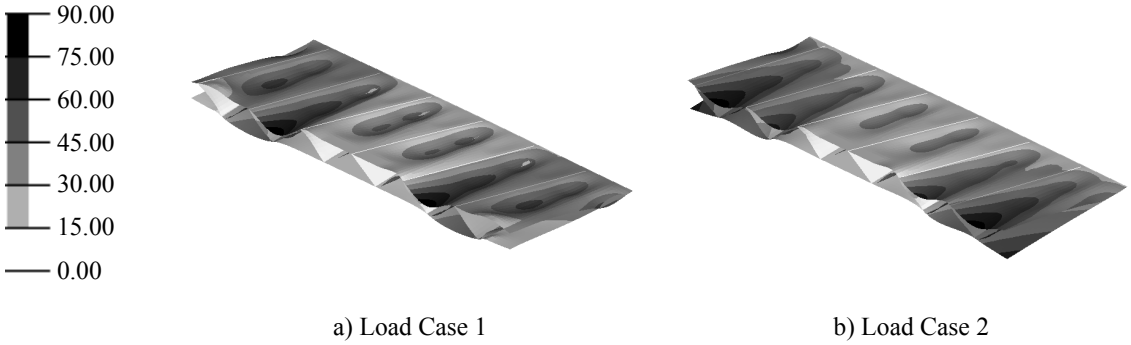

Figure 5: Absolute deformation plot of the zig-zag structure for a) load case 1 and b) load case 2 in $[\mathrm{mm}]$, scale factor: 1.

3.1 Monolithic box with zig-zag stiffeners

The first concept is inspired by structures made from trusses. In such constructions, diagonal trusses are used to produce frames with high resistance to shear forces. Here, the function of a diagonal truss is adopted with plane stiffeners arranged in inclined positions to form a zig-zag pattern as presented in Fig. 4a. A structure designed in this way can be manufactured in one component and one curing process. The overall dimensions are identical to the sandwich structure. The detail dimensions of the zig-zag pattern can be found in Fig. 4b. With $\alpha \approx 35°$ twelve ribs are added as indicated. A distance of $20\ \mathrm{mm}$ between the run-out of one rib and the onset of the next rib is defined to account for design radii needed for manufacturing purpose. The structure is divided along the x-direction (Fig. 1) in three equidistant zones with different ply layup sequences labeled **A**, **B** and **C** (Fig. 4a). The zone-based ply definition can be found in Tab. 3.

The finite element analysis for this design shows large displacements (see Fig. 5), especially at the upper skin and low buckling load factors at the lower skin (see Fig. 6). Regarding the global displacement, listed in Tab. 4, the values for the characteristic nodes 1 and 2 (Fig. 3) are approximately equal to the simplified sandwich structure. The large displacements at node 3 seem to be a result of the missing stiffness against flexural shear at the open end of the structure. Moreover, the local displacements of the upper skin sections between the inclined ribs caused by the externally acting air pressure are unacceptably high. Again, a main portion is caused by the open design at the leading edge. The lower skin sections (parts of the lower

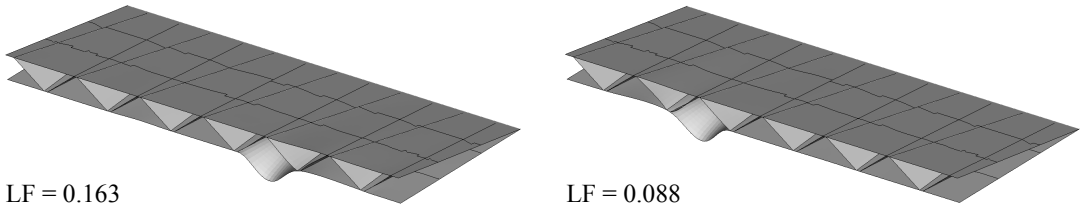

a) Load Case 1 b) Load Case 2

Figure 6: Buckling shapes of the zig-zag structure for a) load case 1 and b) load case 2, scale factor: 100.

skin confined between two inclined ribs) are loaded by in-plane compression and in-plane shear. Thus, this structural elements are prone to buckling and due to the free edge, the risk of buckling is significantly increased. Therefore, the first buckling mode occurs at the leading edge location at very low buckling load factors of 0.163 and 0.088 for load case 1 and load case 2, respectively. These factors multiplied with the limit load show the load level at which buckling occur and should be larger than one. One option to increase the buckling load is to apply additional layers of carbon. However, a high number of plies is needed, because of the currently small load factor. Also other buckling modes, at other locations might become critical. Thus, this approach results in a non-efficient, i.e. not weight optimal structure. The same happens, when the upper skin thickness is increased locally until the displacements caused by the air pressure are reduced to an acceptable limit. Therefore, global design adjustments are necessary to achieve a weight-optimized result, which is actually competitive to the sandwich structure.

3.2 Monolithic torque box with ribs

The obvious solution is to close the open structure. Thereby, the buckling load is increased significantly and the displacements of the local upper skin sections are reduced as the flexural and shear stiffness are increased. This design update can be realized by inserting a C-spar as presented in Fig. 7a to the cost of a separate component needed to be manufactured. However, the complexity of the C-spar is relatively low and the assembly procedure is simple compared to the benefits provided. The C-spar contributes essentially to the global stiffness of the structure, whereas the impact on the mass is low, because of the decreased length of the inclined ribs. The increase in the global stiffness behavior is used to further improve the design regarding buckling and local deformation. The introduced C-spar allows to change the ribs from inclined ones to simply vertical ones as presented in Fig. 7. That means the width of the local upper and lower skin sections are nearly reduced by half in comparison to the zig-zag structure presented in Fig. 4, which has a major impact on buckling and local displacements. The reduced surface of the ribs decreases the resulting mass further.

Finally, the carbon ply layup of the structure is optimized. The standard layup defined by the sandwich structure is applied again. However, it is adjusted with additional plies locally according to the occurring buckling modes. The number of plies and their orientations depend on the principal normal stress. The ply layup of the structure is categorized by zones, which are shown in Fig. 8. The layup sequences of the individual labeled zones are provided in Tab. 3.

As shown in Fig. 8a the layup of zones on the lower skin is the most complex one. These zones are with higher number of plies, resulting in a larger laminate thickness than those on the upper skin. The highest number of plies is needed in the center bracket area (see Fig. 2). The number of plies decreases towards the trailing edge (from $x = 0$ to $x = 800\,\mathrm{mm}$), the

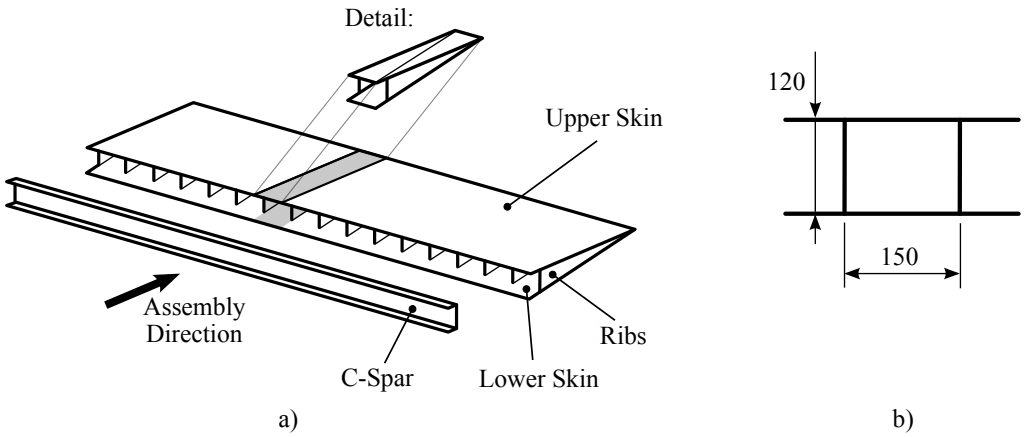

Figure 7: Monolithic torque box with a) ribs and b) its local dimensions in [mm].

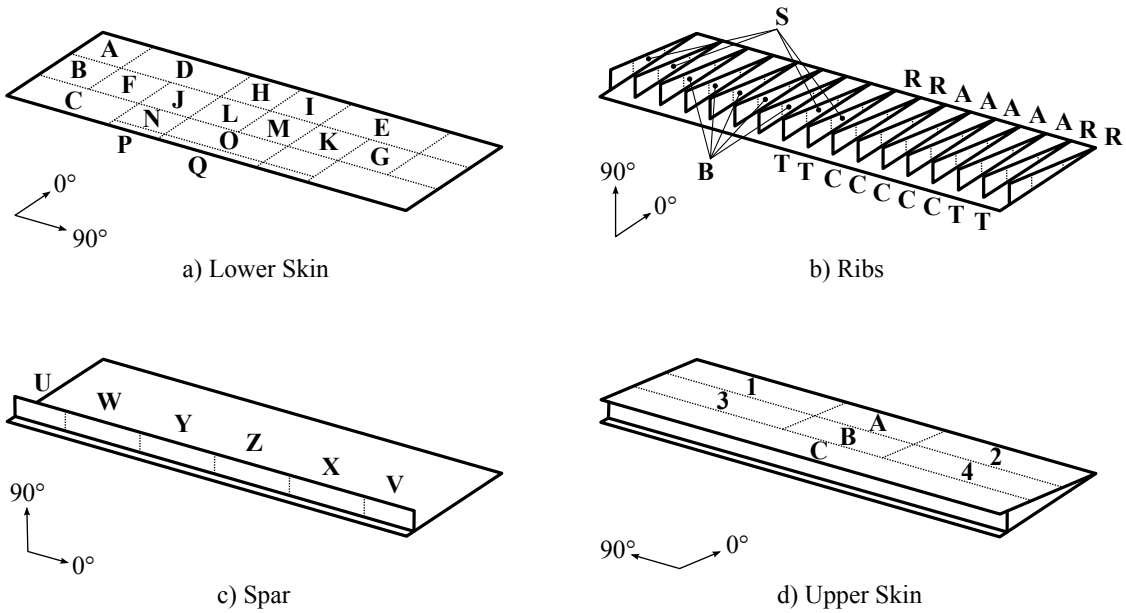

Figure 8: Zone based definition for ply layup sequence of the torque box structure. Not labeled zones are equal to the opposite ones.

Zone	Qty.	Ply Layup
A	6	(45/-45/90/90/-45/45)
B	10	(45/-45/90/90/90/90/90/90/-45/45)
C	14	(45/-45/90/90/90/90/90/90/90/90/90/90/-45/45)
D	8	(45/-45/90/45/45/90/-45/45)
E	8	(45/-45/90/-45/-45/90/-45/45)
F	11	(45/-45/90/90/90/45/90/90/90/-45/45)
G	11	(45/-45/90/90/90/-45/90/90/90/-45/45)
H	9	(45/-45/90/45/0/45/90/-45/45)
I	9	(45/-45/90/-45/0/-45/90/-45/45)
J	12	(45/-45/90/90/90/90/45/90/90/90/-45/45)
K	12	(45/-45/90/90/90/90/-45/90/90/90/-45/45)
L	13	(45/-45/90/90/90/90/45/0/90/90/90/-45/45)
M	13	(45/-45/90/90/90/90/-45/0/90/90/90/-45/45)
N	16	(45/-45/90/90/90/90/90/90/90/90/90/90/90/90/-45/45)
O	17	(45/-45/90/90/90/90/90/90/0/90/90/90/90/90/90/-45/45)
P	24	(45/90/90/90/90/90/-45/45/-45/90/90/90/90/90/90/90/90/90/90/90/90/90/-45/45)
Q	24	(45/90/90/90/90/90/-45/45/-45/90/90/90/90/90/90/0/90/90/90/90/90/90/-45/45)
R	4	(45/-45/-45/45)
S	8	(45/-45/90/90/90/90/-45/45)
T	12	(45/-45/90/90/90/90/90/90/90/90/-45/45)
U	6	(45/-45/-45/-45/-45/45)
V	6	(45/-45/45/45/-45/45)
W	8	(45/-45/-45/-45/-45/-45/-45/45)
X	8	(45/-45/45/45/45/45/-45/45)
Y	10	(45/-45/-45/-45/-45/-45/-45/-45/-45/45)
Z	10	(45/-45/45/45/45/45/45/45/-45/45)
1	8	(45/-45/90/-45/-45/90/-45/45)
2	8	(45/-45/90/45/45/90/-45/45)
3	11	(45/-45/90/90/90/-45/90/90/90/-45/45)
4	11	(45/-45/90/90/90/45/90/90/90/-45/45)

Table 3: Ply layup sequence for the individual zones.

outboard edge and the inboard edge. Except the standard layup the ply sequence is mirrored along the xz-plane of the defined coordinate system given in Fig. 1. The structural mass of the final design is provided in Tab. 7 and is 520 g less than the sandwich structure.

The aforementioned torque box structure is analyzed with respect to displacement, buckling, and static strength. The absolute displacements under applied load cases are shown in Fig. 9 with a scale factor of 5. The displacements of the characteristic nodes can be found in Tab. 4. In general, the displacements are considered to be acceptable. Figures 10a and b present the first buckling mode for load cases 1 and 2, respectively. For both load cases the reserve factors are above 1. The reserve for load case 1 is 1.126 and is thus large enough. The reserve factor 1.001 for load case 2 yields a small margin. However, load case 2 occurs due to failed brackets and for such failure load cases onset of buckling below limit load might be acceptable (when certain conditions, which shall not be discussed here, are fulfilled). For the analysis of the stresses the same procedure as for the sandwich structure is applied. In Tab. 5 the maximum occurring in-plane ply stresses are summarized. For those, the reserve factors for first ply failure according to the maximum stress criteria in (1) are calculated and provided in Tab. 6. As one can see all reserve factors are greater than 1.

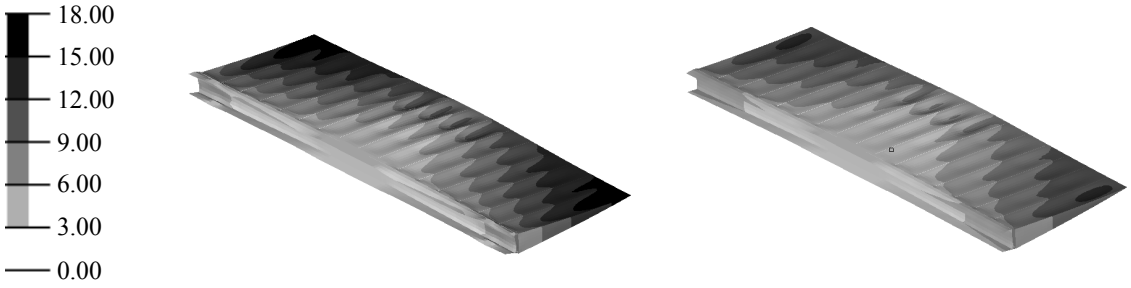

a) Load Case 1 b) Load Case 2

Figure 9: Absolute displacement plot of the torque box structure for a) load case 1 and b) load case 2 in $[\mathrm{mm}]$, scale factor: 5.

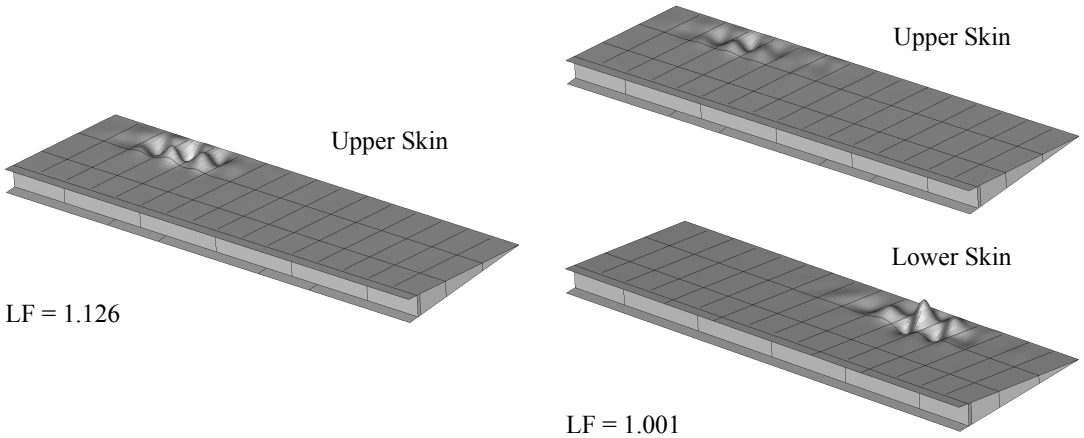

a) Load Case 1 b) Load Case 2

Figure 10: Buckling shapes of the torque box structure for a) load case 1 and b) load case 2, scale factor: 100.

4 DISCUSSION OF RESULTS

Tables 4 to 7 compare the properties of the presented designs. An overview about the global stiffness behavior is given in Tab. 4 on behalf of the three characteristic nodes selected in Fig. 3. The absolute node displacements of the torque box structure are only larger at node 3 for load case 1 and at node 1 for load case 2. However, it seems reasonable to envelope both load cases and consider the maximum displacement of each node only. Therefore, the torque box structure is clearly the better design. The differences in the displacements between the torque box design and the sandwich structure are considerable large. As mentioned in section 3.1, the global stiffness of the zig-zag structure is, except at node 3, approximately in the same range as the sandwich structure, making itself a competitive design in terms of the global stiffness. With respect to the occurring stresses and the resulting reserve factors, the values from the sandwich design and the torque box design are provided only. The stresses in the zig-zag structure are not further discussed here because of the unacceptable large deflections. Table 5 presents the maximum occurring in-plane ply stresses for load cases 1 and 2, respectively. The stress values are approximately the same for load case 1, whereas the stress values of the torque box structure for load case 2 are less than half of those from the sandwich structure. This result is remarkable.

	Node 1	Node 2	Node 3
Load Case 1			
Sandwich Structure	10.41	17.84	1.52
Zig-Zag Structure	10.57	18.59	24.39
Torque Box Structure	8.75	15.85	2.37
Load Case 2			
Sandwich Structure	1.00	17.94	17.47
Zig-Zag Structure	6.56	13.78	28.21
Torque Box Structure	5.50	11.65	5.45

Table 4: Absolute displacement of the alternative designs at the three characteristic nodes, [mm].

	σ_{11}^t	σ_{11}^c	σ_{22}^t	σ_{22}^c	σ_{12}
Load Case 1					
Sandwich Structure	492.5	519.9	38.7	40.4	25.3
Torque Box Structure	546.4	518.4	39.7	40.0	23.6
Load Case 2					
Sandwich Structure	795.7	821.7	34.0	35.1	32.2
Torque Box Structure	362.4	259.9	20.3	14.4	12.6

Table 5: Maximum in plane ply stresses for the alternative designs for load cases 1 and 2 in [MPa].

A conclusion with respect to the strength of the sandwich and torque box structure is made in Tab. 6 for load cases 1 and 2. Here, the resulting reserve factors in accordance with the maximum stress requirement given in (1) are provided. Finally, the structural mass of each design is calculated. The results and their details are stated in Tab. 7. As one can see, the mass of the torque box structure is 520g less than the mass of the sandwich structure. For the zig-zag structure a mass reserve of 1.01kg to the sandwich structure exists, which could be used for structural improvements.

5 CONCLUSION

In this work a path towards the substitution of a honeycomb core in a sandwich structure by a structure entirely made from carbon plies was presented. Two major external (i.e. not geometrical) requirements on the structure were considered and finally realized. These were on the one hand, the integration of a lower skin for aerodynamic reasons and on the other hand, the manufacturing in a single layup and curing process (with exception of an assembly step for a pre-produced C-spar afterwards).

As expected, the critical design requirement moved from material strength to structural stability. The honeycomb core, which supports the lower and upper skin as a distributed foundation

	RF_{11}^t	RF_{11}^c	RF_{22}^t	RF_{22}^c	RF_{12}
Load Case 1					
Sandwich Structure	5.3	2.8	1.4	7.1	4.2
Torque Box Structure	4.8	2.8	1.4	7.1	4.4
Load Case 2					
Sandwich Structure	3.3	1.8	1.6	8.1	3.3
Torque Box Structure	7.2	5.6	2.7	19.8	8.3

Table 6: Minimum reserve factor for the alternative designs for load cases 1 and 2.

	Carbon	Core	Adhesive	Total
Sandwich Structure	4.64	5.53	0.94	11.11
Zig-Zag Structure	10.10	-	-	10.10
Torque Box Structure	10.52	-	0,07	10.59

Table 7: Mass calculation of the design alternatives, [kg].

was replaced by local skin supports in the form of applied ribs and a C-spar. Consequently, the skins became critical for buckling in the sections between the supports. In addition, the need to close the structure were justified, because this measure increased the buckling load factor and reduced the local skin section deformations essentially. The mass equivalent (or even better, the reduced mass) substitution of the sandwich structure was in principal realized after introduction of closing the geometry to act as a torque box.

The presented designs are introduced on basic analytical considerations in a step-by-step approach. First, the global layout was defined by uniformly distributed ribs. Then, the ply numbers, orientations and layup sequences were adjusted according to iteratively calculated results of deformation and buckling analyses. Finally a stress analysis was performed to assure the compliance with the material allowables. However, the possibility of irregular distributed stiffeners together with a locally optimized laminate thickness was not addressed in this article and is part of future investigations.

REFERENCES

[1] M. Meindlhumer, M. Schagerl and M. Fleischmann, *Towards a monolithic design of large aircraft wing spoilers using numerical topology and laminate optimization*. In: Rodrigues et al. (Eds.): Engineering Optimization IV, 651-656, Taylor and Francis Group, London, 2015.

[2] M. C. Y. Niu, *Airframe structural design - Practical design information and data on aircraft structures, 2nd Edition*. Hong Kong Comilit Press Ltd., 2002.

[3] CS-25 Amendment 3, *Certification specifications for large aeroplanes*. EASA, 2007.

[4] E. J. Barbero, *Introduction to composite materials design, 2nd Edition*. Taylor and Francis Group LLC, 2011.